HHS Public Access

Author manuscript

IEEE Access. Author manuscript; available in PMC 2024 July 09.

Published in final edited form as:

IEEE Access. 2023 ; 11: 143998–144005. doi:10.1109/access.2023.3343637.

Investigating Local Receive Arrays in tcMRgFUS System and Their Influence by Passive Antennas: A Simulation Study

MING LU[1,2], **XINQIANG YAN**[1,2,3] **[Member, IEEE]**

[1]Vanderbilt University Institute of Imaging Science, Vanderbilt University Medical Center, Nashville, TN 37232, USA

[2]Department of Radiology and Radiological Sciences, Vanderbilt University Medical Center, Nashville, TN 37232, USA

[3]Department of Electrical and Computer Engineering, Vanderbilt University, Nashville, TN 37232, USA

Abstract

Transcranial magnetic resonance-guided focused ultrasound (tcMRgFUS) revolutionizes non-invasive therapy by combining MRI and high-intensity focused ultrasound for precise thermal treatment. MRI scans play an essential role during tcMRgFUS treatment in that they are used to localize the target and monitor temperature. Using the body coil for MRI introduces imaging challenges, notably extremely low signal-to-noise ratio (SNR) and a distinct dark band in 3 Tesla brain images. This study explores the impact of diverse local receive coils on SNR and parallel imaging capabilities in tcMRgFUS. Simulation results underscore the significant SNR enhancement, especially with helmet-shaped coils, crucial for capturing signals from the head's top and sides. Additionally, the study delves into integrating passive antennas to address the dark band issue, revealing a combined improvement in SNR and transmit field recovery. The study demonstrates that even a coil array outside the water bath can enhance SNR. This work offers critical insights into optimizing the imaging quality, improving temperature mapping accuracy, and recovering the transmit field in tcMRgFUS technology, holding potential for refined treatment visualization, targeting precision, and real-time monitoring.

Keywords

Focused ultrasound; interventional MRI; passive antenna; RF coils; electromagnetic simulations

I. INTRODUCTION

Transcranial magnetic resonance-guided focused ultrasound (tcMRgFUS) is a non-invasive and targeted therapeutic technique that has gained increasing attention recently. This

Corresponding author: Xinqiang Yan (xinqiang.yan@vumc.org).

The associate editor coordinating the review of this manuscript and approving it for publication was Guido Lombardi 0000-0002-7311-2279.

innovative technology combines magnetic resonance imaging (MRI) and high-intensity focused ultrasound (HIFU) to precisely deliver thermal energy to specific brain regions, allowing for non-invasive treatment of various neurological conditions. This technology is effective in treating essential tremors, Parkinson's disease, and neuropathic pain, among other conditions [1], [2], [3].

MRI is crucial during the tcMRgFUS treatment [4], [5], [6]. High imaging quality in MRI is essential for accurately localizing the target tissue and monitoring the real-time procedure of focused ultrasound (FUS) treatment. This is crucial for optimizing treatment parameters and ensuring the FUS is applied precisely to the intended area. Additionally, MRI monitors temperature changes in tissues during FUS treatments. The ability to accurately measure temperature changes in real-time is vital for controlling and adjusting the intensity of the FUS to achieve the desired therapeutic effects while minimizing damage to surrounding healthy tissue. Furthermore, accurate MRI imaging helps avoid unintended damage to critical structures, reducing the risk of side effects or complications. This is particularly important in treating conditions where precision is paramount, such as FUS neuromodulation.

Signal-to-noise (SNR) is a fundamental parameter in MRI that directly impacts the quality and accuracy of images. SNR is inversely proportional to the spatial resolution. Higher SNR allows for improved spatial resolution, enabling the visualization of smaller structures and finer details in the imaged area. Higher SNR also improves the accuracy, precision, and speed of real-time temperature mapping. In the default MRgFUS system, the body coil was used for both transmission and reception, and as a result, the MR imaging quality was not fully optimized.

Recently, efforts have been made to improve the imaging quality and temperature mapping accuracy in the tcMRgFUS system by incorporating local receive coils [7], [8], [9], [10]. Jones et al. developed a 2-channel local receive-only coil array, with a similar version now commercially available [7], [9]. This two-channel coil, also called the 'Princess Leia' coil, consists of loop coils placed on each side of the head (by the ears). It demonstrated an SNR improvement of approximately four times at the brain's center [9]. The coil is designed to be submerged in a water bath to align its center with the brain center to maximize SNR in this region. The 2-channel coil is encased in a silicone membrane and integrated into the membrane that contains the coupling water inside the transducer to prevent water leakage.

In addition to the 2-channel array, other designs with more elements have been proposed. Corea et al. introduced a 4-channel screen-printed coil array that exhibits approximately four times the SNR improvement at the surface area and twice the SNR improvement at the center of a gel phantom compared to the body coil [8]. Saniour et al. induced an 8-channel AIR coil and reported a significant SNR improvement compared to the body coil [10].

Although receive coils with different numbers of elements have been investigated, these coils are all arranged in a single row and do not cover the top of the head. It is well known that a helmet-shaped coil is optimal for brain imaging as it can capture the MR signal from both the top and sides of the head. The multi-row helmet shape is the standard

design for receive arrays in modern MRI scanners [11], [12], [13]. This study delves into the performance of a multi-row helmet receive array as well as single-row arrays.

Currently, the ExAblate Neuro (Insightec, Haifa Israel) is the only commercial and FDA-approved system for tcMRgFUS neurosurgery, with over 120 system installations as of September 2022 [14]. In this system, however, there is a curved dark band in brain images that runs through midbrain locations targeted for ablation treatment. This dark band was caused by the destructive interference between the incoming RF wave from the body coil and the reflected RF wave owing to the conductive transducer bowl [15], [16], [17]. Besides the degradation in the MRI signal reception, this destructive interference also leads to extremely low efficiency and severe inhomogeneity of the RF transmit field. The mentioned local coils cannot solve such issues in RF transmission as they are for receive-only purposes. Hadley et al. and Yan et al. demonstrated that the passive ground reflector [18] or passive wires/antennas in the ‘Propeller Beanie’ configuration can significantly alleviate the dark band phenomenon and recover the transmit field [15], [16], [17].

To fully realize the potential of tcMRgFUS and enable high-power RF pulses, such as diffusion imaging, to monitor the treatment, the passive ‘Propeller Beanie’ antenna design or a similar one is still needed. Therefore, it would be helpful to determine whether the ‘Propeller Beanie’ antenna can be combined with the local receive arrays to maximize both the transmit and receive RF performance of the Insightec tcMRgFUS system. In this work, we first compare the receive performance of different coils in terms of coil tuning/matching, SNR and parallel imaging capability, and then investigate how the passive antennas affect the coil performance.

II. METHODS

A. PASSIVE CROSSED WIRES/ANTENNAS

Before detailing the simulation method, let us briefly revisit the mechanism of the dark band issue in the Insightec tcMRgFUS and the passive crossed wires/antennas method that mitigates this problem. The tcMRgFUS device has a 30-cm diameter hemispherical transducer bowl to ensure the ultrasound beam can be focused on the region of interest. Because the scanner’s built-in body coil used for MRI excitation sits outside the transducer, the RF transmit signal (incoming electromagnetic wave) that interacts with the brain for MRI mainly comes from the transducer’s bottom opening. This is due to the shielding effect of the transducer bowl, preventing direct passage of the electromagnetic wave. Meanwhile, the bowl’s hemispherical shape and the conductive surface make it similar to a circular dish reflector. This dish reflector generates reflected waves and, thus, a secondary field. At approximately a quarter wavelength from the top of the bowl, the reflected waves are out of phase with the incoming waves, and the secondary and original fields interfere destructively, as illustrated in Figure 1A. This leads to the transmit field null and the corresponding dark band. Since the transducer bowl is filled with water (high permittivity dielectric), the effective quarter wavelength is around 7 cm. Unfortunately, the dark band runs through the brain’s center, as Figure 1B shows.

Owing to the principle of reciprocity [19], this dark bank exists for both transmit and receive RF fields if the body coil is utilized for both transmission and reception. Even if the local receive coil is used for reception, such a dark band still manifests in the transmit field, leading to imaging artifacts [9]. As mentioned above, the signal cancellation or the imaging dark band is caused by the destructive interference between the reflected and incoming waves [17]. Therefore, it can be avoided if the reflected wave does not destructively interfere with the incoming wave. One straightforward solution is adding an artificial reflector between the head and the bowl/shield to manipulate the reflected wave. This reflector is preferably transparent to the ultrasonic beams and easily fabricated. Inspired by the Yagi-Uda antenna [20], Yan et al. introduced a pair of orthogonal dipole antennas as an artificial reflector to control the reflected wave [17]. The dark band could be alleviated or even avoided by setting the length of dipole antennas to 11cm, as shown in Figure 1C.

Based on the analysis of the mechanism of the dark band, it is possible to use metamaterials-inspired resonators, such as massive period wires [21], [22], to control the reflected wave and alleviate the dark band. However, future studies are required to investigate whether such designs can recover the RF field in MRI and whether they disturb the ultrasound beams from transducers.

B. ELECTROMAGNETIC SIMULATION

This study investigates four kinds of receive coil arrays. The first array is a 2-channel design resembling the commercially available ‘Princess Lisa’ coil [7], [9]. Each coil has a circular shape with a diameter of 15 cm, half submerged in the water bath to ensure the coil’s center is allied with the center of the brain, referred to as the ‘2-ch submerged array’ (Figure 2B). The second is a 6-channel design resembling the volume-type receive arrays [8], [10]. Like the 2-channel array, half of the 6-channel array is submerged in the water bath, referred to as the ‘6-ch submerged array’ (Figure 2D). Each coil has a square shape and dimensions of 10 cm ×10 cm. These six coils are evenly distributed along the circumference of an ellipse (25 cm × 19 cm) to match the curved surface of the human head model. The third array is a 6-channel design of the same size and layout, with all coils entirely outside the water bath, referred to as the ‘6-ch outside array’ (Figure 2C). Such a design is preferred from an engineering perspective since it eliminates concerns about water leakage or coil instability. The fourth array is a 12-channel design with dual rows and a helmet shape, referred to as the ‘12-ch submerged array’ (Figure 2E). In this array, coils in the bottom row have the exact sizes and layouts as those of 6-ch arrays, while coils in the top row are trapezoidal and bent to form a helmet shape, matching the anatomical shape of the top of the human head. As a baseline comparison, we also simulated a body coil (16-rungs, high-pass birdcage), which has a length of 70 cm and a diameter of 60 cm (Figure 2A).

All these coils were investigated in two scenarios: without the passive antennas (Figures 2A–2E) and with the passive antennas (Figures 2F–2J). Passive antennas are made of 11-cm-long and 1-mm-diameter copper wires in a ‘Propeller Beanie’ configuration [17]. These wires were intentionally arranged orthogonally without any physical connection, maintaining a separation of 1.5 mm between them. They were enveloped in insulation

composed of 0.07-mm-thick polyester to mimic an AWG-18 non-magnetic copper wire (specifically, Belden 8076 magnet wire).

The following simulations were performed to assess the potential impact of passive antennas on coil impedance matching. First, the coils were tuned to 128 MHz (Larmor frequency of the 3 Tesla scanner) and matched 50 Ω without passive antennas. Subsequently, they were re-evaluated without retuning or rematching in the presence of the passive antennas. The coil conductors were modeled using copper, and the capacitors were modeled considering the equivalent resistance. The relative permittivity and conductivity of water were set to 81 and 0.01, respectively, to replicate the typical tap water used in practice.

All simulations were performed with a Finite Element Method (FEM)-based Maxwell solver (Ansys HFSS, Canonsburg, PA, USA). The electrical and magnetic field data were exported to MATLAB for the calculation of the SNR and geometry (g-) factor. A vendor-provided human model (Ansys HFSS, Canonsburg, PA, USA) comprising more than 33 organs and 330 tissues was employed. The electromagnetic (EM) and RF co-simulation method (along with Ansys Designer) was used to accelerate the simulation process and to ensure accuracy [23], [24], [25].

C. SNR AND G-FACTOR CALCULATION

The reception field of each coil element (B_1^-) was calculated using Equation (1), where B_x and B_y are transverse RF magnetic fields [26]. The sample noise matrix (R_s) was calculated by integrating the power dissipation over the entire sample volume, as shown in Equation (2). Here E_{km} is the local electric field of voxel k from coil element m, E_{kn} is the local electric field of voxel k from coil element n, Δx, Δy, and Δz are the voxel size in x, y, and z directions, receptivity [27]. The voxel size was set to 2 mm × 2 mm × 2 mm in this study.

The coil noise matrices (R_c), including the conductor noise and component noise, were calculated by integrating power dissipation over all conductors (P_{cond}) and all components (P_{compon}), as shown in Equation (3) [28]. SNR is proportional to the ratio between the B_1^- and the total noise and is evaluated using Equation (4). Another critical factor in assessing a receive array is its ability to complement the reduced gradient encoding of parallel imaging. The g-factor, influencing the SNR in the accelerated images, depends on the number and geometrical configurations of the array elements, as calculated by Equation (5) [29].

$$B_1^- = (B_x - i B_y)^*/2 \tag{1}$$

$$R_s = \Delta x \Delta y \Delta z \times \sum\nolimits_k \sigma_k \left(E_{km} E_{kn}^* \right) \tag{2}$$

$$R_c = \oiint (P_{cond} + P_{compon}) \tag{3}$$

$$SNR \propto \sqrt{B_1^{-H} \times (R_s + R_c) \times B_1^-} \tag{4}$$

$$g_j = \sqrt{\left[\left(E_R^\dagger \Psi^{-1} E_R\right)\right]_{j,j} \left[\left(E_R^\dagger \Psi^{-1} E_R\right)^{-1}\right]_{j,j}} \tag{5}$$

III. RESULTS

A. INFLUENCE ON COIL IMPEDANCE BY PASSIVE WIRE/ANTENNA

The top and bottom rows of Figure 3 plot the reflection coefficients (S11) of coils without and with the presence of passive antennas [17], respectively. As previously mentioned, all coils were tuned and matched at 128 MHz, with S_{11} less than −20 dB, indicating a return loss of less than 1%.

For all single-row receive arrays (2)-ch submerged, 6-ch submerged, and 6-ch outside arrays), there are minimal changes in the S_{11} plots in the presence of passive antennas, with the worst S_{11} still less than −15 dB (i.e., <2% return loss). This implies that coil tuning and matching could be well preserved, eliminating the need to retune or rematch the coils when combined with passive antennas. This is particularly important for routine coils as they are typically not feasible for users to adjust the components. We believe this preservation is partly due to passive antennas acting as dipoles with a different field pattern than the loop coils and also because the passive antennas are positioned at a considerable distance from the coils.

However, it is observed that several coils in the top row of the 12-channel array exhibit impedance mismatching and resonate frequency shifts when the passive antennas are added. This could be attributed to the close proximity between the antennas and these coils, resulting in non-negligible mutual coupling and subsequent changes in coil impedance. Therefore, tuning and matching coils in the presence of passive antennas is recommended if both the dual-row and passive antennas are employed.

B. CURRENT DISTRIBUTION

Figures 4 A–D and 4 E–G show the current distribution of individual coil elements for different arrays without and with passive antennas, respectively. Induced currents are observed on the passive antenna parallel to the coil plane when one top coil is excited. According to the principle of reciprocity, this antenna could be seen as an extension of the

coil and would alter the receive sensitivity or SNR pattern. Interestingly, the passive antenna perpendicular to the coil plane exhibits fewer induced currents when the coil is excited.

For the top row coils of the dual-row array, the induced current on the passive antenna is even stronger than that of the excited coil due to their strong coupling. Such findings align with the S-parameter results in Figure 3.

C. SIMULATED SNR AND G-FACTOR

Figure 5 presents the simulated SNR maps in the central coronal planes. SNR was normalized to make the central SNR for the body coil (without passive antennas) equal 1. One of the main targets in tcMRgFUS treatments is the thalamus, which is located in the center of the brain [30]. Table 1 lists the central SNR values of various coil arrays and the percentage of SNR change when adding passive antennas. The central SNR was averaged over the 3-cm-diameter circular area at the brain's center, as shown in the white circle in Figure 5.

Compared to the body coil, the 2-ch submerged coil exhibits approximately 4.2 times SNR improvement, consistent with previous findings [9]. The 6-ch submerged coil shows about 6 times SNR improvement compared to the body coil. Compared to the 2-ch coil, it has 1.4 times more SNR improvement due to its volume structure, capable of capturing signals in both left-right and anterior-posterior directions. This is also consistent with the fact that a quadrature coil exhibits a $\sqrt{2}$ SNR increase compared to a linear coil [31], [32], [33]. Surprisingly, we noted that the central SNR could be improved by up to ~12 times compared to the body coil when using a close-fitting dual-row helmet coil, which is still twice the improvement compared to a 6-channel single-row submerged coil. The top coils play a crucial role in the SNR at the central brain owing to their close-fitting geometry. In Li et al. [34], a single top coil contributes more to the central SNR than multiple surrounding MRgFUS coils. Besides these submerged coils, we also noted that the outside 6-ch coil could achieve 2.7 times SNR improvement compared to the body coil, as receive sensitivity slightly extends beyond the coil's physical size, covering the central brain to some extent.

For these single-row arrays, adding passive antennas can enhance the central SNR by 15% to 24%. This improvement is attributed to the passive antennas acting as extensions of the coils, as also validated in Figure 4, enabling them to capture MR signals from both the top and sides of the head.

For the dual-row helmet array, however, there is an SNR drop in the presence of passive antennas. This is partly because the top coils in the dual-row array already cover the top of the head, and partly because the passive antennas slightly affect the coil noise correlation. Nevertheless, the SNR decrease caused by the passive antennas is still negligible (9%) and does not hinder their use in improving the transmit performance.

The body coil alone could be the scenario using the default coil setting in current tcMRgFUS system. The 2-ch submerged array could be seen as the scenario using the existing commercially available coil [9], and the 6-ch submerged array could be seen as the scenario using the existing local coil array designs [8], [10].

Figure 6 shows the g-factor maps for different coil arrays without and with passive antennas in the sagittal plane, with acceleration factors (R) from 1 to 3. The g-factor represents the fraction of the SNR obtained compared to the case of no acceleration in the SENSE reconstruction. In general, arrays with more elements yield lower g-factors. The impact of passive antennas on the g-factor is minimal for the 2-channel and 6-channel arrays. For the 12-channel dual-row array, the passive antennas increase the g-factor when R is up to 3. As mentioned above, this could be attributed to the coupling of passive antennas with the coils in the 12-channel array, making the coil receive profile less distinct.

IV. DISCUSSIONS

Most tcMRgFUS systems still utilize the body coil for MRI signal reception. In this work, we extensively investigated the receive performance of different local receive coils in the tcMRgFUS system. Our numerical results align with previous studies that the local coils could significantly improve the SNR [7], [8], [9], [10] and be incorporated into practical implementations. Furthermore, our findings indicate that a multi-row helmet array, which is also a standard local head coil array in MRI, exhibits an even higher SNR (approximately two times) and better parallel imaging performance than single-row arrays. This highlights a considerable opportunity to enhance imaging quality in tcMRgFUS, particularly for capturing MRI signals from the top of the head, crucial for SNR at the center of the brain, which single-row arrays cannot effectively capture.

Another critical aspect of this work is the investigation of these coils in conjunction with passive ‘Propeller Beanie’ antennas [17]. As mentioned earlier, local receive coils alone cannot solve the low transmit efficiency at the center of the brain and severe transmit field inhomogeneity, although they improve the SNR. Combining passive antennas with local receive coils is necessary to maximize imaging quality in tcMRgFUS. Importantly, our findings indicate that the passive antennas do not compromise the receive performance of local arrays. In most cases, they enhance the central SNR. Even in the dual-row array, where coils in the top row are close to the passive antennas, there is only a slight SNR drop, negligible in practical applications.

Several engineering challenges exist for practical local coils, especially those submerged in the water bath. First, these coils must go through the membrane, requiring a specific solution to prevent water leakage. For example, the commercial 2-channel coil integrates a disposable rubber membrane to avoid water leakage [9]. Second, considering that treatments often last several hours, the stability of submerged coils in water must be considered [8]. In some applications where submerged coils are impractical, the outside coil might be preferable. Our simulation results reveal that an outside array, along with the passive antennas, could achieve a 2.7-time SNR improvement compared to the default body coil. It should also be noted that this work is focused on the RF coil design itself and does not consider its interference with the ultrasound beam. However, several groups have demonstrated that RF coils could be highly transparent to ultrasonic energy by using thin wire conductors [35] or screen-printed conductors [8], [36].

V. CONCLUSION

In conclusion, our comprehensive investigation of different local receive coil arrays in tcMRgFUS and their combination with passive ‘Propeller Beanie’ antennas offers valuable insights and guidance for practical RF coil designs to maximize both the RF receive and transmit performance. The SNR improvement using advanced local receive coil arrays will be immediately helpful in essential tremor treatments through better visualization and improved targeting of regions of interest, such as the thalamus. Furthermore, higher SNR allows for greater spatial precision and increased temporal resolution in MR thermometry, paving the way to multi-slice and volumetric thermometry. Lastly, recovering the transmit field would enable spin-echo RF pulses, such as diffusion-weighted imaging, which can potentially improve lesion conspicuity, and FGATIR, which can improve the accuracy of anatomical segmentation. Future work should focus on fabricating the dual-row local receive array, using it along with the passive antenna in clinical treatments, and assessing their impact on intra-operative targeting, thermal evaluation, lesion assessment and scan time during MRgFUS.

Acknowledgments

This work was supported by NIH under Grant R21 EB 029639.

Biographies

MING LU received the B.S. degree from Lanzhou University, Lanzhou, China, in 2009, and the Ph.D. degree from Beijing Normal University, Beijing, China, in 2014. In 2019, he was a Visiting Scholar with Vanderbilt University, Nashville, TN, USA. He is currently an Associate Professor with the College of Nuclear Equipment and Nuclear Engineering, Yantai University, Yantai, Shandong, China. His current research interests include MRI RF coil electromagnetic analysis and design. This work was done during his visit to Vanderbilt University.

XINQIANG YAN (Member, IEEE) received the Ph.D. degree in particle physics and nuclear physics from the Institute of High Energy Physics, Chinese Academy of Sciences, in 2014. He joined the Radiofrequency (RF) Laboratory, Institute of Biophysics, Chinese Academy of Sciences, in 2011, where he developed RF coils and RF/analog circuits for 7 T and 9.4 T scanners. At the end of 2014, he moved to the Vanderbilt University Institute

of Imaging Science, as a Postdoctoral Research Fellow. In 2016, he joined the Vanderbilt Faculty, as a Research Instructor. He is currently a Research Associate Professor with the Department of Electrical Engineering and Computer Science, Vanderbilt University, and the Department of Radiology, Vanderbilt University Medical Center. His research interests include enhancing RF and B_0 homogeneity, expediting acquisition speed, mitigating motion artifacts, and amplifying the signal-to-noise ratio. His research pursuits revolve around the advancement of engineering solutions aimed at addressing the technical hurdles encountered in the realms of MRI. He was a recipient of the IEEE IMWS-BIO Best Student Paper Award in 2013 and the Summa Cum Laude Award and Magna Cum Laude Award of ISMRM.

REFERENCES

[1]. McDannold N, "Quantitative MRI-based temperature mapping based on the proton resonant frequency shift: Review of validation studies," Int. J. Hyperthermia, vol. 21, no. 6, pp. 533–546, Sep. 2005, doi: 10.1080/02656730500096073. [PubMed: 16147438]

[2]. McDannold N, Clement GT, Black P, Jolesz F, and Hynynen K, "Transcranial magnetic resonance imaging-guided focused ultrasound surgery of brain tumors: Initial findings in 3 patients," Neurosurgery, vol. 66, no. 2, pp. 323–332, Feb. 2010, doi: 10.1227/01.neu.0000360379.95800.2f. [PubMed: 20087132]

[3]. Elias WJ, Huss D, Voss T, Loomba J, Khaled M, Zadicario E, Frysinger RC, Sperling SA, Wylie S, Monteith SJ, Druzgal J, Shah BB, Harrison M, and Wintermark M, "A pilot study of focused ultrasound thalamotomy for essential tremor," New England J. Med, vol. 369, no. 7, pp. 640–648, Aug. 2013, doi: 10.1056/nejmoa1300962. [PubMed: 23944301]

[4]. Rieke V, Vigen KK, Sommer G, Daniel BL, Pauly JM, and Butts K, "Referenceless PRF shift thermometry," Magn. Reson. Med, vol. 51, no. 6, pp. 1223–1231, Jun. 2004, doi: 10.1002/mrm.20090. [PubMed: 15170843]

[5]. Rieke V and Butts Pauly K, "MR thermometry," J. Magn. Reson. Imag, vol. 27, no. 2, pp. 376–390, Feb. 2008, doi: 10.1002/jmri.21265.

[6]. Holbrook AB, Santos JM, Kaye E, Rieke V, and Pauly KB, "Real-time MR thermometry for monitoring HIFU ablations of the liver," Magn. Reson. Med, vol. 63, no. 2, pp. 365–373, Feb. 2010, doi: 10.1002/mrm.22206. [PubMed: 19950255]

[7]. Jones M, Hadley JR, Minalga E, Snell J, Hananel A, and Eames M, "Improving MR image quality for FUS treatments: Initial results from an ultrasound-compatible RF coil," in Proc. Focused Ultrasound 3rd Int. Symp, Washington, DC, USA, vol. 2012, p. 123.

[8]. Corea J, Ye P, Seo D, Butts-Pauly K, Arias AC, and Lustig M, "Printed receive coils with high acoustic transparency for magnetic resonance guided focused ultrasound," Sci. Rep, vol. 8, no. 1, p. 3392, Feb. 2018, doi: 10.1038/s41598-018-21687-1. [PubMed: 29467432]

[9]. Bitton RR, Sheingaouz E, Assif B, Kelm N, Dayan M, Butts Pauly K, and Ghanouni P, "Evaluation of an MRI receive head coil for use in transcranial MR guided focused ultrasound for functional neurosurgery," Int. J. Hyperthermia, vol. 38, no. 1, pp. 22–29, Jan. 2021, doi: 10.1080/02656736.2020.1867242. [PubMed: 33459092]

[10]. Saniour I, Robb FJL, Taracila V, Mishra V, Vincent J, Voss HU, Kaplitt MG, Chazen JL, and Winkler SA, "Characterization of a low-profile, flexible, and acoustically transparent receive-only MRI coil array for high sensitivity MR-guided focused ultrasound," IEEE Access, vol. 10, pp. 25062–25072, 2022, doi: 10.1109/ACCESS.2022.3154824. [PubMed: 35600672]

[11]. Wiggins GC, Triantafyllou C, Potthast A, Reykowski A, Nittka M, and Wald LL, "32-channel 3 Tesla receive-only phased-array head coil with soccer-ball element geometry," Magn. Reson. Med, vol. 56, no. 1, pp. 216–223, Jul. 2006, doi: 10.1002/mrm.20925. [PubMed: 16767762]

[12]. de Zwart JA, Ledden PJ, van Gelderen P, Bodurka J, Chu R, and Duyn JH, "Signal-to-noise ratio and parallel imaging performance of a 16-channel receive-only brain coil array at 3.0 Tesla," Magn. Reson. Med, vol. 51, no. 1, pp. 22–26, Jan. 2004, doi: 10.1002/mrm.10678. [PubMed: 14705041]

[13]. de Zwart JA, Ledden PJ, Kellman P, van Gelderen P, and Duyn JH, "Design of a SENSE-optimized high-sensitivity MRI receive coil for brain imaging," Magn. Reson. Med, vol. 47, no. 6, pp. 1218–1227, Jun. 2002, doi: 10.1002/mrm.10169. [PubMed: 12111969]

[14]. (Sep. 1, 2022). Insightec Announces Financing up to $200 Million to Fund Continued Growth. Accessed: May 4, 2023. [Online]. Available: https://www.bloomberg.com/press-releases/2022-09-01/insightec-announces-financing-up-to-200-million-to-fund-continued-growth

[15]. Yan X and Grissom WA, "Passive wire reflectors for improved image quality in MR-guided focused ultrasound," US Patent 20 200 360 733 A1, Nov. 19, 2020. Accessed: Mar. 1, 2023. [Online]. Available: https://patents.google.com/patent/US20200360733A1/en

[16]. Yan X, Allen SP, and Grissom WA, "Propeller" beanie passive antennas to alleviate dark bands in transcranial MR-guided focused ultrasound," in Proc. Annu. Meeting ISMRM, 2020, p. 113.

[17]. Yan X, Allen S, Lu M,Moore D, Meyer CH, and Grissom WA, "Dark band artifact in transcranial MR-guided focused ultrasound: Mechanism and mitigation with passive crossed wire antennas," Magn. Reson. Imag, vol. 103, pp. 169–178, Nov. 2023, doi: 10.1016/j.mri.2023.07.018.

[18]. Hadley JR, Odéen H, Merrill R, Adams SI, Rieke V, Payne A, and Parker DL, "Improving image quality in transcranial magnetic resonance guided focused ultrasound using a conductive screen," Magn. Reson. Imag, vol. 83, pp. 41–49, Nov. 2021, doi: 10.1016/j.mri.2021.07.002.

[19]. Hoult DI, "The principle of reciprocity," J. Magn. Reson, vol. 213, no. 2, pp. 344–346, Dec. 2011, doi: 10.1016/j.jmr.2011.08.005. [PubMed: 21889377]

[20]. Yagi H, "Beam transmission of ultra short waves," Proc. Inst. Radio Eng, vol. 16, no. 6, pp. 715–740, Jun. 1928, doi: 10.1109/JRPROC.1928.221464.

[21]. Hurshkainen A, Nikulin A, Georget E, Larrat B, Berrahou D, Neves AL, Sabouroux P, Enoch S, Melchakova I, Belov P, Glybovski S, and Abdeddaim R, "A novel metamaterial-inspired RF-coil for preclinical dual-nuclei MRI," Sci. Rep, vol. 8, no. 1, Jun. 2018, Art. no. 1, doi: 10.1038/s41598-018-27327-y.

[22]. Motovilova E and Huang SY, "Hilbert curve-based metasurface to enhance sensitivity of radio frequency coils for 7-T MRI," IEEE Trans. Microw. Theory Techn, vol. 67, no. 2, pp. 615–625, Feb. 2019, doi: 10.1109/TMTT.2018.2882486.

[23]. Kozlov M and Turner R, "Fast MRI coil analysis based on 3-D electromagnetic and RF circuit co-simulation," J. Magn. Reson, vol. 200, no. 1, pp. 147–152, Sep. 2009, doi: 10.1016/j.jmr.2009.06.005. [PubMed: 19570700]

[24]. Yan X, Ma C, Shi L, Zhuo Y, Zhou XJ, Wei L, and Xue R, "Optimization of an 8-Channel loop-array coil for a 7 T MRI system with the guidance of a co-simulation approach," Appl. Magn. Reson, vol. 45, no. 5, pp. 437–449, May 2014, doi: 10.1007/s00723-014-0526-6.

[25]. Yan X, Cao Z, and Zhang X, "Simulation verification of SNR and parallel imaging improvements by ICE-decoupled loop array in MRI," Appl. Magn. Reson, vol. 47, no. 4, pp. 395–403, Apr. 2016, doi: 10.1007/s00723-016-0764-x. [PubMed: 27034578]

[26]. Hoult DI, "The principle of reciprocity in signal strength calculations A mathematical guide," Concepts Magn. Reson, vol. 12, no. 4, pp. 173–187, 2000, doi:10.1002/1099-0534(2000)12:4<173::AID-CMR1>3.0.CO;2-Q.

[27]. Cao Z, Oh S, Sica CT, McGarrity JM, Horan T, Luo W, and Collins CM, "Bloch-based MRI system simulator considering realistic electromagnetic fields for calculation of signal, noise, and specific absorption rate," Magn. Reson. Med, vol. 72, no. 1, pp. 237–247, Jul. 2014, doi: 10.1002/mrm.24907. [PubMed: 24006153]

[28]. Lu M, Gore JC, and Yan X, "Over-overlapped loop arrays: A numerical study," Magn. Reson. Imag, vol. 72, pp. 135–142, Oct. 2020, doi: 10.1016/j.mri.2020.07.006.

[29]. Pruessmann KP, Weiger M, Scheidegger MB, and Boesiger P, "SENSE: Sensitivity encoding for fast MRI," Magn. Reson. Med, vol. 42, no. 5, pp. 952–962, 1999. [PubMed: 10542355]

[30]. Jameel A, Gedroyc W, Nandi D, Jones B, Kirmi O, Molloy S, Tai Y, Charlesworth G, and Bain P, "Double lesion MRgFUS treatment of essential tremor targeting the thalamus and posterior sub-thalamic area: Preliminary study with two year follow-up," Brit. J. Neurosurgery, vol. 36, no. 2, pp. 241–250, Mar. 2022, doi: 10.1080/02688697.2021.1958150.

[31]. Chen C-N, Hoult DI, and Sank VJ, "Quadrature detection coils–A further √2 improvement in sensitivity," J. Magn. Reson, vol. 54, no. 2, pp. 324–327, Sep. 1983, doi: 10.1016/0022-2364(83)90057-4.

[32]. Hoult DI, Chen C-N, and Sank VJ, "Quadrature detection in the laboratory frame," Magn. Reson. Med, vol. 1, no. 3, pp. 339–353, Sep. 1984, doi: 10.1002/mrm.1910010305. [PubMed: 6571563]

[33]. Hayes CE, Edelstein WA, Schenck JF, Mueller OM, and Eash M, "An efficient, highly homogeneous radiofrequency coil for whole-body NMR imaging at 1.5 T," J. Magn. Reson, vol. 63, no. 3, pp. 622–628, Jul. 1985.

[34]. Li Y, Lee J, Long X, Qiao Y, Ma T, He Q, Cao P, Zhang X, and Zheng H, "A magnetic resonance-guided focused ultrasound neuromodulation system with a whole brain coil array for nonhuman primates at 3 T," IEEE Trans. Med. Imag, vol. 39, no. 12, pp. 4401–4412, Dec. 2020, doi: 10.1109/TMI.2020.3019087.

[35]. Köhler MO, Tillander M, Syrjä A, Nakari R, and Ylihautala M, "Ultrasound-transparent RF coil design for improved MR thermometry of HIFU therapy," in Proc. ISMRM, 2011, p. 1728.

[36]. Corea JR, Flynn AM, Lechêne B, Scott G, Reed GD, Shin PJ, Lustig M, and Arias AC, "Screen-printed flexible MRI receive coils," Nature Commun, vol. 7, no. 1, Mar. 2016, doi: 10.1038/ncomms10839.

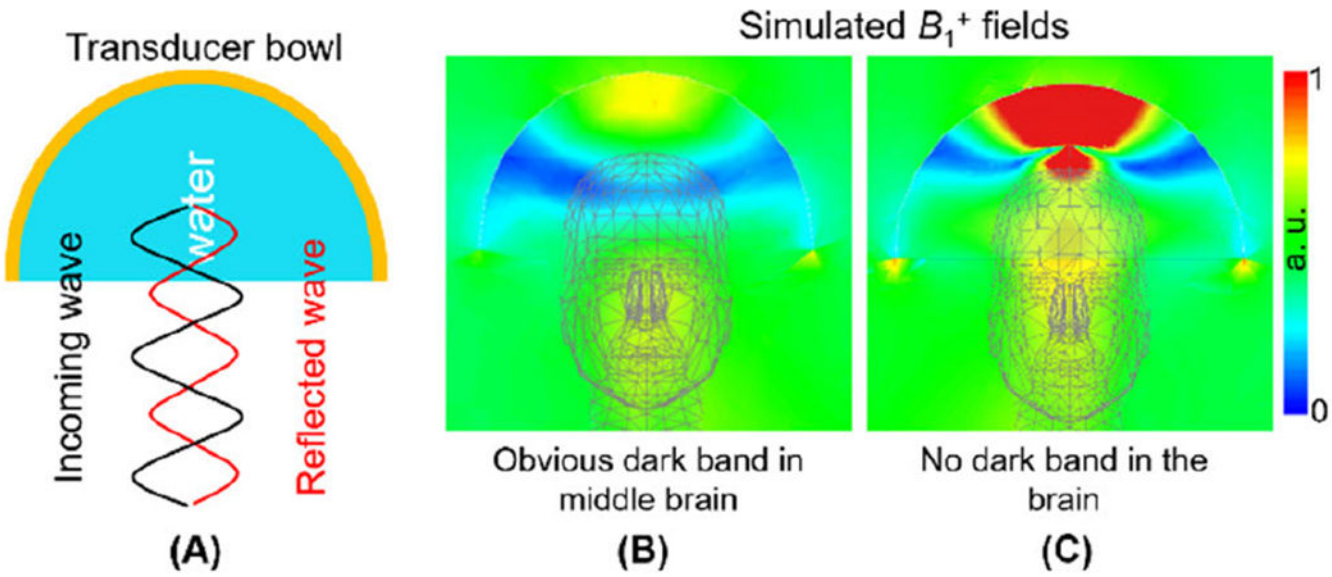

FIGURE 1.

A: Illustration of the destructive interference between the incoming and reflected EM signals. B and C: Simulated transmit field (B_1^+) at a human model without and with the passive crossed wires/antennas [16].

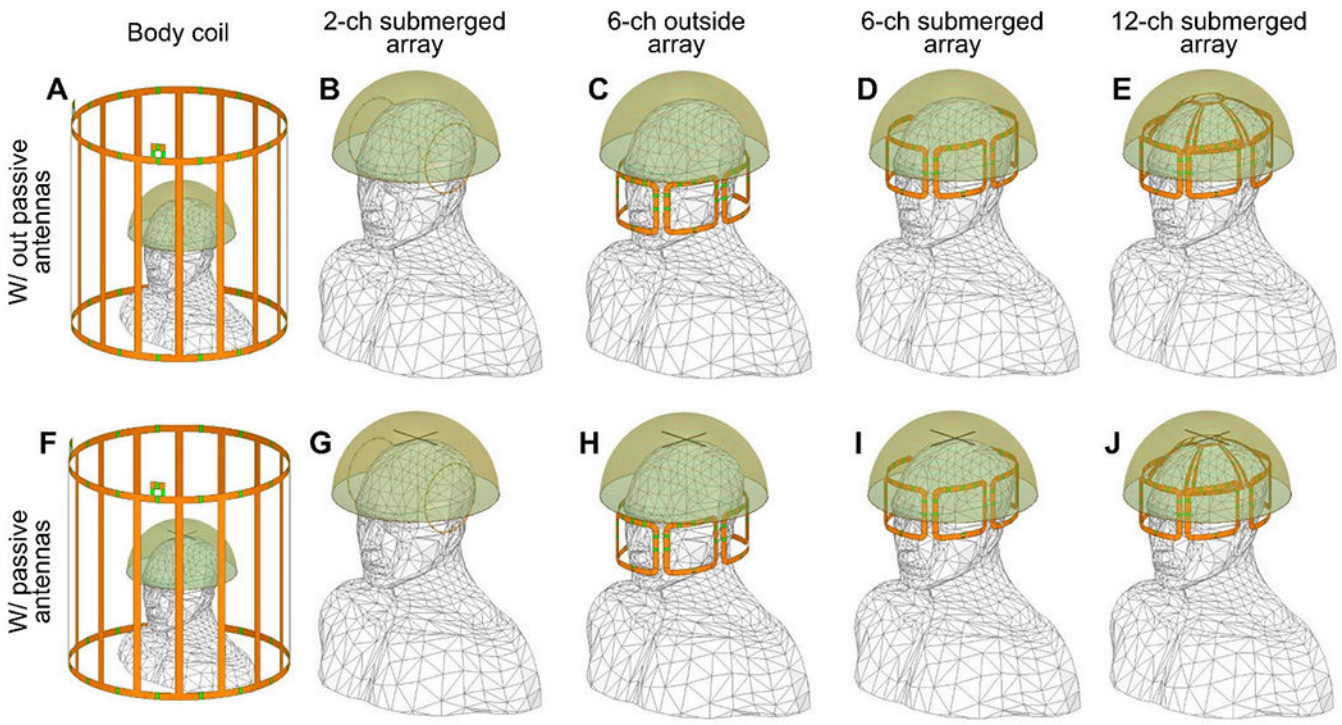

FIGURE 2.

A and F: Simulation models of body coil alone in tcMRgFUS system without and with passive antennas. B-E: Simulation models of different local receive coil arrays without passive antennas. G-J: Simulation models of these receive arrays with passive antennas. The passive antennas have a length of 11 cm and are arranged in a ‘Propeller Beanie, following the previous work [17].

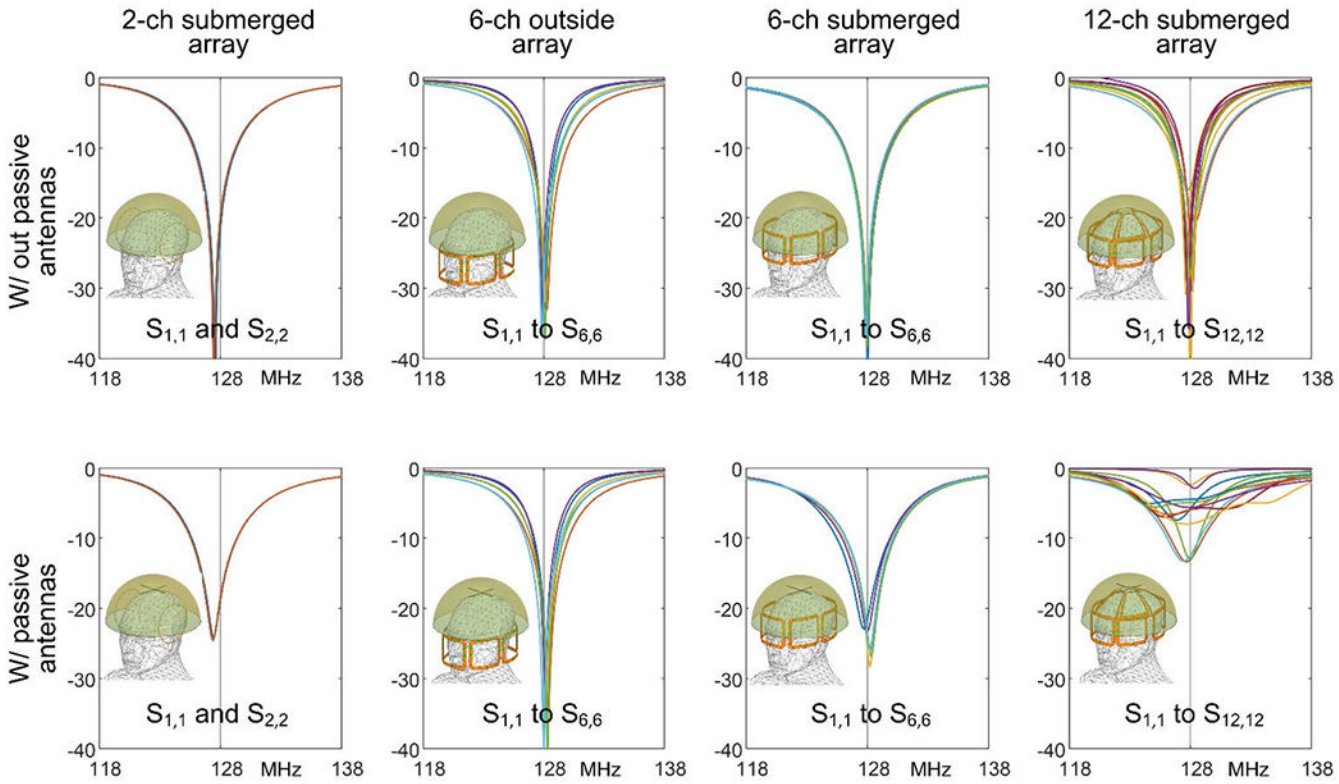

FIGURE 3.

Comparison of coil impedance matching (or return loss, S_{11}) for different local receive arrays without and with passive antennas. From left to right: 2-ch submerged array, 6-ch outside array, 6-ch submerged array, and 12-ch submerged array.

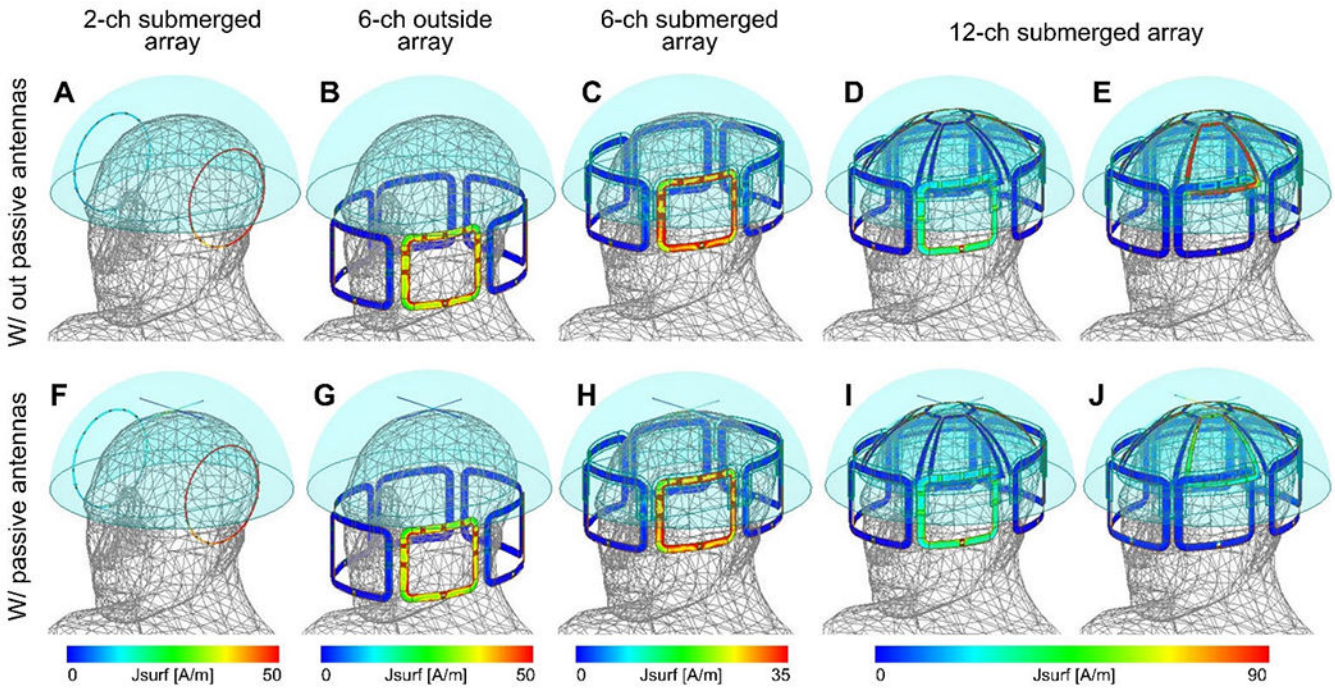

FIGURE 4.

Simulation surface current distribution on coils and passive antennas. From left to right: 2-ch submerged array, 6-ch outside array, 6-ch submerged array, and 12-ch submerged array. For each scenario, only one coil was excited with a united power, with all other coils terminated with 50 Ω. The top coil and bottom coil in the dual-row array have different influences on the passive antennas, so they were both investigated.

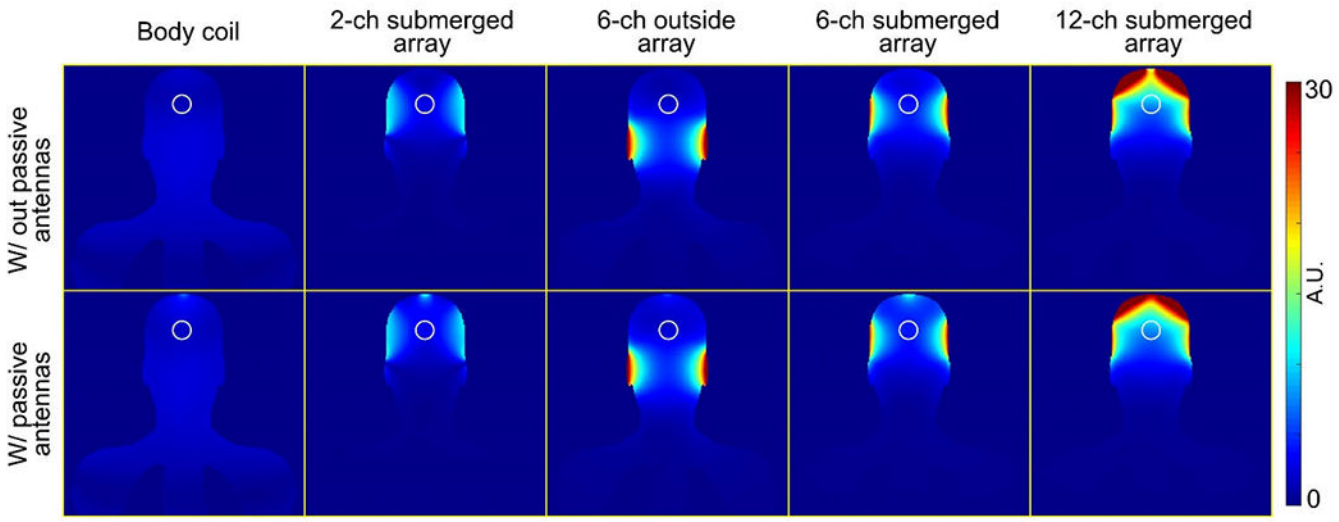

FIGURE 5.

Simulated coronal SNR maps for different coils without (top row) and with (bottom row) the presence of passive antennas [17]. From left to right: body coil, 2-ch submerged array, 6-ch outside array, 6-ch submerged array, and 12-ch submerged array. Central SNR values were averaged over a 3-cm-diameter circular area (marked in white). SNR was calculated from Eqs. 1–4 and normalized to make the central SNR for the body coil (without passive antennas) equal 1.

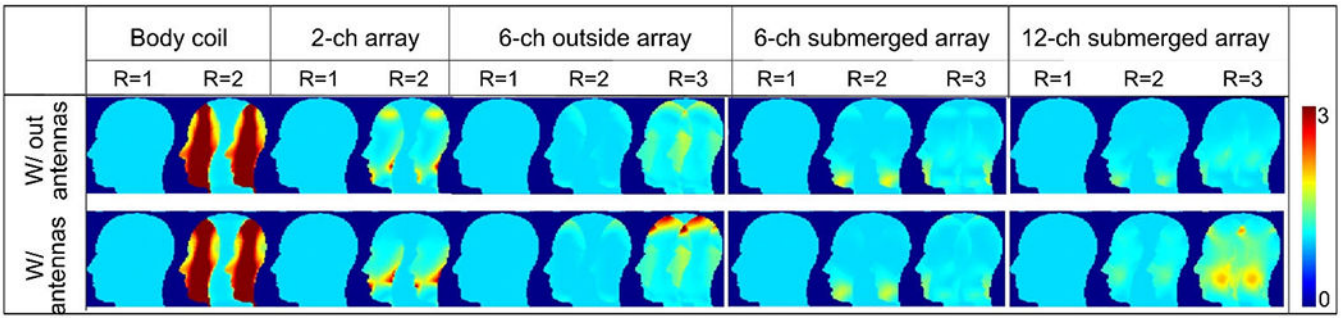

FIGURE 6.

Simulated g-factor maps for different coils without (top row) and with (bottom row) the presence of passive antennas. From left to right: 2-ch submerged array, 6-ch outside array, 6-ch submerged array, and 12-ch submerged array.

TABLE 1.

The central SNR values of various coil arrays and the percentage of SNR change when using passive antennas.

Simulated SNR	Body coil	2-ch submerged array	6-ch outside array	6-ch submerged array	12-ch submerged array
Without cross wire	1.0	4.2	2.7	6.0	11.2
With cross wire	2.1	5.2	3.1	7.3	10.2
Increase	+110%	+24%	+15%	+21%	−9%